JAST
Journal of Aerospace Science and Technology

Pages: 146-158 / Vol. 16/ No. 1 /Winter- Spring 2023

Journal of Aerospace Science and Technology

www:jast.ias.ir

Scienctifie-Research Article

Improving the Performance and Work-Absorbing Capacity of the Axial-Flow Compressor by Using Tandem Blades

Alireza Sekhavat Benis[1], **Reza Aaghaei-Togh**[2]*
1-2- Department of Aerospace Engineering, Science and Research Branch, Islamic Azad University, Tehran, Iran

ABSTRACT

Keywords: *Compressor, Rotor, Tandem, Compressor Characteristics, Performance Improving, Work Absorption.*

The compressor blade is responsible for increasing the flow pressure. By adding a blade behind the main blade, the compressor performance can be improved by increasing the pressure ratio and reducing the weight. The tandem improves the performance and increases the compressor absorption coefficient by increasing the pressure ratio, preventing flow separation and controlling the boundary layer. This has led compressor designers to seek the reduction in weight, and increase in the pressure ratio as well as efficiency by employing a tandem. The geometry of the compressor blade and stage along with its tandem has been obtained from previous valid sources and has been drawn in three dimensions and numerically analyzed. Then various parameters for the blade and tandem are examined separately and the pressure and velocity vectors are plotted to illustrate the control of the vortices, and the improvement of compressor performance. Finally, the characteristic curve of the compressor and the pressure ratio for this particular tandem are plotted. Calculations show that by using the tandem and removing the excess vortex after the main blade, a 28.5% increase in total pressure, a 15% decrease in relative Mach number and a 1.5% decrease in entropy is seen

Introduction

Holding a secondary blade to, and immediately after the main blade in a turbomachine is called a tandem. The presence of the tandem, increases the pressure ratio in one compressor stage, thus reducing the total number of stages. By dividing the applied load between the main blade and the tandem blade, the flow rotation rate in a compressor stage increases, in a way that a higher-pressure ratio can be achieved in each stage. As the pressure ratio increases, the performance of the compressor stage is expected to increase, respectively. In the blade and tandem set which are studied in this work, the applied load is divided equally.

Also, the tandem blade prevents flow separation by controlling the boundary layer. In this way, the main effect of employing tandem blades is to increase the load on the compressor stage and, as a result, reduce the weight of the engine by making the compressor assembly smaller.

A literature view on some of the previous studies on tandem blades, are reviewed below.

1 PhD. Candidate
2 Assistant Professor (Corresponding Author) **Email:** : reza_tog@srbiau.ac.ir

DOI : 10.22034/jast.2022.357363.1126
Submit: 22.08.2022 / Accepted: 11.12.2022
Print ISSN:1735-2134 Online ISSN: 2345-3648

Saha and Roy [1], experimentally investigated the performance of the tandem compressor vane row at low speeds in the wind tunnel by using 3 blade types: (a) simple airfoil blades, (b) blades with tandem, and (c) blades with redesigned tandem airfoils. Among the available airfoils, the ones suitable to use in the tandem blade row were introduced. Mesgarpour Tousi et al. [2] investigated a tandem compressor stage as a transient numerical solution and studied the differences between steady and transient solutions. They showed that the transient solution predicts the performance range of the tandem stage by about 25% in the design stage, and about 28% in the 80% milestone. Then, they studied the flow mechanism and aerodynamic structure affecting the instability of the flow inside the stage.

Eftari et al. [3] investigated the flow losses of an axial compressor, numerically and experimentally, at different speeds and pressure ratios. They used different computational and experimental methods to calculate the loss in the compressor and finally reached the conclusion that Lieblin, Koch Smith and Howell models are more accurate than other methods. Carstens [4] developed a coupling simulation method to study the displacement of the motion stability boundary, which is caused by the strong flow separation effect and the fluctuation of shocks. Using this method, the fluctuation behaviour (flutter) of the blade row is investigated through the moving computing network. This research showed that the compressor rotor has a linear aeroelastic behaviour in design conditions, and was later used to check the tandem floor in flutter and aero-acoustic modes.

McGlumphy et al. [5] numerically analysed the subsonic flow on the axial compressor tandem blade. This analysis was done for an axial compressor without shock and the numerical analysis was done based on the position of the normal and tandem blade. This study shows that stage with a tandem has a better performance for the off-design mode. McGlumphy et al. [6], investigated the performance of tandem blades of an axial compressor as well as Lieblin's loss model based on the applied load, by using two-dimensional numerical analysis. The tandem rotor is seen to have a far better performance compared to the normal rotor. McGlumphy et al. [7] analysed the tandem airfoil for an axial compressor's core in a three-dimensional way and compared the performance of a tandem included stage as well as a normal stage. They observed that the tandem included stage has a much better performance and a more stable performance interval.

Zadoski [8] used the coupling method for the three-dimensional simulation of the flow in a five-and-a-half-staged compressor for a transonic flow. He was able to obtain temporal resonances as well as existing vibrations by using fluid-structure interaction for the studied compressor. He used the finite volume method in three-dimensions to calculate the structural part. Rajadurai [9] investigated the low-speed flow for a tandem compressor rotor and compared the interaction between the main blade and the tandem with the performance of a normal blade. Mohsen et al. [10] studied the effect of using the NASA Rotor 37 tandem blade on the rotor performance in a transonic flow (with Mach 1.4) by two-dimensional numerical method. They concluded that the tandem blade increases the flow rotation without separation and thus increases the pressure ratio by 17% and the adiabatic efficiency of the rotor by 2%.

Pan et al. [11] investigated the optimal design of a tandem blade in a supersonic flow for rotor 37 and studied the secondary flow as well as the shock wave after the blade. Investigations showed that the mass flow rate and the safe range of operation (surge range) increase. They also observed that the efficiency is escalates by 1.6% and the surge margin is increased by 2.75%. The main reason for this improvement is the reduction of the three-dimensional flow effects, by optimizing the tandem, resulting in the optimal distribution of the impinging flow from the escape edge of the rotor tandem to the attack edge of the stator, hence reducing the three-dimensional effects significantly. Droshenko et al. [12] numerically investigated the aero-acoustic parameters of a single-stage compressor with tandem and listed its advantages. They came to the conclusion that with the use of tandem blades, the compressor pressure ratio increased between 1 and 15% (8.5% at the design point) and the acoustic efficiency increased significantly.

Liu et al. [13] employed tandem blades to increase the amount of load applied to the axial compressor. They defined the parameter E (the ratio of increase in static pressure at the design point to the maximum increase in static pressure) as the limit of the compressor stall based on theoretical models, which indicates the ability of tandem compressor to increase the applied load limit. By experimentally comparing the normal class with

the tandem class, they found that the efficiency improvement was 1% and the stall limit improvement was 6%. Babu et al. [14] studied the secondary vortices of a tandem rotor for the axial compressor. Due to the increase in the flow energy by using a tandem, it lowers the discreteness and increases the amount of rotation of the flow on the suction surface of the blade. This flow rotation after the rotor causes a separation at the beginning of the stator. The flow in different time steps was investigated using the limited stream lines and the surface of separated areas and the explosion of vortices. The results showed that new vortices are formed by mixing the rotor vortices with the stator attack edge. As can be seen, the use of tandem blades in axial compressors has significant positive effects; But it is still necessary to investigate in more detail the effect of this type of blade on the performance of the compressor, especially in conditions outside the design point. In the present work, the results of the tandem blade effect on the performance of one stage of a specific axial compressor in the design conditions and outside the design point have been investigated, and its effect on the work absorption coefficient, as a representative of the compressor's overall performance, has been studied.

Geometry of the problem

The geometry used in this study is the model studied at NASA Lewis Research Center [15]. Geometry specifications are presented in Table No. 1:

Table 1. Geometric specifications of rotor and tandem.

Title	Amount
Rotor tip diameter	30 inches
Tip to root ratio	0.7 to 0.8
Rotor tip loss coefficient	Less than 0.55
The rigidity of the rotor tip	1.4 to 1.5

Also, the following should be taken into consideration in geometry:

A) There is no inlet guide vane in the geometry (axial inlet flow).

b) The output of the stator current is axial.

c) The curved surfaces of the blade are in the form of two circular arcs.

It can be concluded that the tandem on the back of the blade is the flap on the wing, and the idea of the tandem may have been taken from the flap. The overall shape of the rotor investigated in this research according to Lewis NASA's research report is shown in Figure 1 and the geometric characteristics of the tandem floor are shown in Table 2.

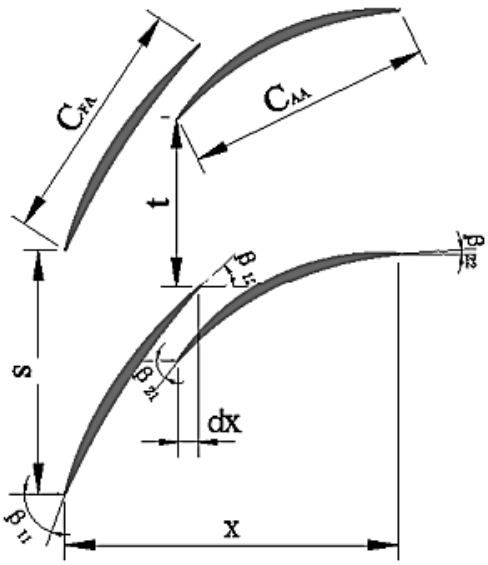

Figure 1. The geometry of the studied tandem Stage.

Table 2 Geometric specifications of tandem-included stage.

Title	Equation
Front airfoil chord	$\varphi_{FA} = \beta_{11} - \beta_{12}$
Rear airfoil chord	$\varphi_{AA} = \beta_{21} - \beta_{22}$
General chord	$\varphi_{OV} = \beta_{11} - \beta_{22}$
Average Chord	$C_{eff} = (1 - 0.5 * \mathrm{AO}) * -$
Effective stiffness	$\sigma_{eff} = C_{eff}/s_{eff}$
Axial overlap	$AO = dx/x$
Step percentage	$PP = t/s$

In the above table, φ is used for the chord calculation, β represents the blade angle, t is the blade thickness, s shows the blade pitch, and indexes 1 and 2 represent blade input and output, respectively.

Then the desired geometry is modelled in three dimensions as shown in Figure 2:

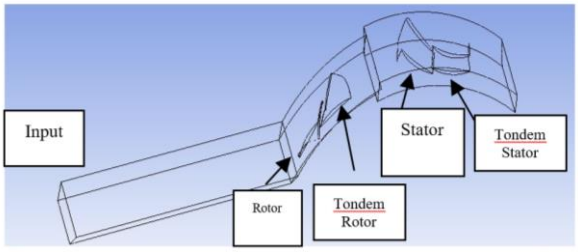

Figure 2. 3D model of the studied geometry.

Governing Equations

For three-dimensional flow modeling, Navier-Stokes equations for compressible flow with Reynolds averaging have been used assuming the following:

$$u = \tilde{u} + u''.H = \tilde{H} + H''$$
$$p = \bar{p} + p'.\rho = \bar{\rho} + \rho'$$

The equations of conservation of mass, momentum and energy are presented in relations 1 to 3, respectively:

Mass:

$$\frac{\partial \bar{\rho}}{\partial t} + \frac{\partial}{\partial x_j}(\bar{\rho}\tilde{u}_j) = 0 \tag{1}$$

Momentum:

$$\frac{\partial}{\partial t}(\bar{\rho}\tilde{u}_j) + \frac{\partial}{\partial x_j}(\bar{\rho}\tilde{u}_i\tilde{u}_j) = -\frac{\partial \bar{p}}{\partial x_i} + \frac{\partial}{\partial x_j}(\bar{\tau}_{ij} - \overline{\rho u_i'' u_j''}) \tag{2}$$

Energy:

$$\frac{\partial}{\partial t}(\bar{\rho}\tilde{H}) + \frac{\partial}{\partial x_j}\left(\bar{\rho}\tilde{u}_j\tilde{H} + \overline{\rho u_i'' H_j''} - k\frac{\partial \bar{T}}{\partial x_j}\right) = \frac{\partial \bar{p}}{\partial t} + \frac{\partial}{\partial x_j}(\tilde{u}_i\,\bar{\tau}_{ij} + \overline{u_i''\tau_{ij}}) \tag{3}$$

It should be noted that the stability analysis has been done and the sentences related to time are removed in all the equations presented in this section.

To model the turbulent flow in turbomachines, there are various models in commercial codes. The turbulence model selection depends a lot on the physics which governs the flow, calculation accuracy, network quality and computing facilities. Two-equation models are more practical than other models. These models provide a good compromise between numerical efforts and computational accuracy. The k-ω model properly predicts the behaviour of the flow near the wall, by using dense elements near the wall [16].

The SST k-ω turbulence equation has been used to model the flow turbulence [16]. Navier's equations must be completed with the equation of state for an ideal gas to close the system of equations. The equation of state for a perfect gas is as follows:

$$p = \rho RT \tag{4}$$

The two-equation models are based on the concept of eddy viscosity.

In the k-ω model, it is assumed that the turbulent viscosity is related to the turbulent kinetic energy as well as the turbulent frequency through equation (5).

$$\mu_t = \rho\frac{k}{\omega} \tag{5}$$

In this method, two transfer equations are solved, one for the perturbed kinetic energy k and the other for the perturbed frequency ω. The stress tensor is calculated from the viscosity-vorticity concept.

$$\frac{\partial(\rho k)}{\partial t} + \frac{\partial}{\partial x_j}(\rho u_j k) = \frac{\partial}{\partial x_j}\left[\left(\mu + \frac{\mu_t}{\sigma_k}\right)\frac{\partial k}{\partial x_j}\right] + P_k - \beta'\rho k\omega + P_{kb} \tag{6}$$

$$\frac{\partial(\rho\omega)}{\partial t} + \frac{\partial}{\partial x_j}(\rho u_j \omega) = \frac{\partial}{\partial x_j}\left[\left(\mu + \frac{\mu_t}{\sigma_\omega}\right)\frac{\partial \omega}{\partial x_j}\right] + \alpha\frac{\omega}{k}P_k - \beta\rho\omega^2 + P_{\omega b} \tag{7}$$

where P_k is the turbulence production rate and the coefficients of this equation are presented in different references.

P_k is the production of turbulence by means of viscous forces and is calculated in the form of equation (8):

$$P_k = \mu_t\left(\frac{\partial u_i}{\partial x_j} + \frac{\partial u_j}{\partial x_i}\right)\frac{\partial u_i}{\partial x_j} - \frac{2}{3}\frac{\partial u_k}{\partial x_k}\left(3\mu_t\frac{\partial u_k}{\partial x_k} + \rho k\right) \tag{8}$$

For incompressible flow, the value of $\partial u_k/\partial x_k$ is small, and the second term on the right side of the above equation does not play an important role in producing turbulence. The value of $\partial u_k/\partial x_k$ for compressible flow is significant only in regions

with high-speed divergence such as shocks. The term $3\mu_t$ in the above equation prevents the values of k and ε from being too large in the shocks. If the full buoyancy model is used, the expression of the buoyancy generation P_{kb} is written as follows:

$$P_{kb} = -\frac{\mu_t}{\rho\sigma_\rho} g_i \frac{\partial \rho}{\partial x_i} \quad (9)$$

Whereas if the Buzinsk model is used, this expression is calculated as follows:

$$P_{kb} = -\frac{\mu_t}{\rho\sigma_\rho} \rho\beta g_i \frac{\partial T}{\partial x_i} \quad (10)$$

A combination of the two models is employed in order to simultaneously make use of their capability in both high and low Reynolds numbers. This model, which is known as the SST method, in many flows, like flows with reverse pressure gradient, works more accurately and reliably [16]. Although this model presents the capabilities of both models, due to the transition from one model to another, it may face instabilities in the solution or deal with a weak convergence. It is noteworthy that considering the mentioned contents, the SST model is used in this research.

Numerical Model

Numerical analysis of 3D flow was done with CFX commercial software. The cell vertex method has been used to discretize the computing environment. Using the Gauss theory, the volume integral is converted into a surface integral, and the averaged Reynolds Navier–Stokes equations on this level are transformed into algebraic equations by integration, which are solved by the implicit method.

One channel is modelled for the rotor and another channel for the stator. As mentioned before, the equations are solved in a stable way. To obtain the performance curve and the floor pressure ratio, the outlet pressure is continuously increased until numerical instability is observed.

The method of applying rotation to the rotor is done using the Multi-Rotating Frame model or MRF.

Boundary conditions

The following boundary conditions have been used for all simulations in this study:

a) The total pressure and temperature are used for the entrance of the floor; so that the total pressure is equal to 1 atmosphere, and the total temperature is equal to 288 Kelvin. At the same time, the direction of the flow in the inlet and outlet is axial.

b) All the walls i.e., blade, shell and root are considered without roughness.

c) The averaged static pressure condition is also used in the output.

Computing network

After generating the geometry of the compressor floor, the computational network was created based on the study of the quality and independence of the network. The rotor pressure ratio parameter is considered to check the independence of the solution from the grid. For this purpose, 6 different computing networks were created and the pressure ratio parameter was evaluated at the design cycle (4210 rpm). According to Table 3, it can be seen that the above parameter has remained almost constant in the last 3 cases (rows 4 to 6); Therefore, in order to reduce the cost of calculations, network 4 with 745621 nodes was selected for study.

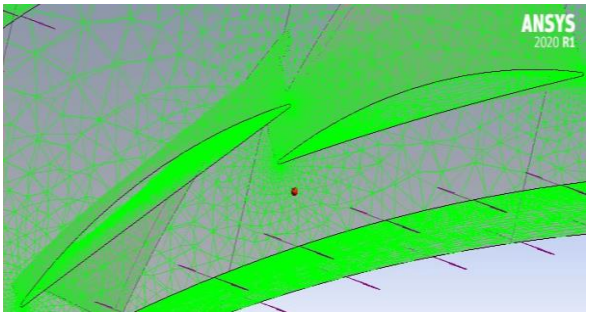

Figure 3. The grid generated for the studied rotor geometry and rotor tandem.

Table 2. The results of the study of network independence

Row	The number of nodes	Rotor pressure ratio
1.	194865	1.1958
2.	335475	1.2152
3.	524899	1.2554
4.	745621	1.2758
5.	896522	1.2786
6.	1212253	1.2789

As it is seen in Table 3, with the increase of the number of nodes, the value of the rotor pressure ratio becomes closer to its original value (1.28) which is also mentioned in the NASA Lewis report [15]. By increasing the number of nodes from rows 1 to 3, a relatively large change in the value of the pressure ratio is observed. But by making it smaller from rows 4 to 6, the rotor pressure ratio

does not change much and remains almost constant.

Validation of the model

In order to validate the obtained results and validate the model, the isentropic efficiency obtained from the laboratory results of NASA's Lewis report [15] is compared with the three-dimensional analysis of the present research, in Figure 4. As it can be seen in figure 4, the numerical and experimental results are in acceptable agreement with each other and the difference is due to the higher flow rate in the numerical results. The flow rate is higher in the numerical analysis compared to the experimental results. It is due to the lower surface friction, compared to the friction in the experiment; as its value is not specified in the reference report [15]. According to the explanations provided, the modelled geometry and applied network have the necessary qualities for the numerical simulation.

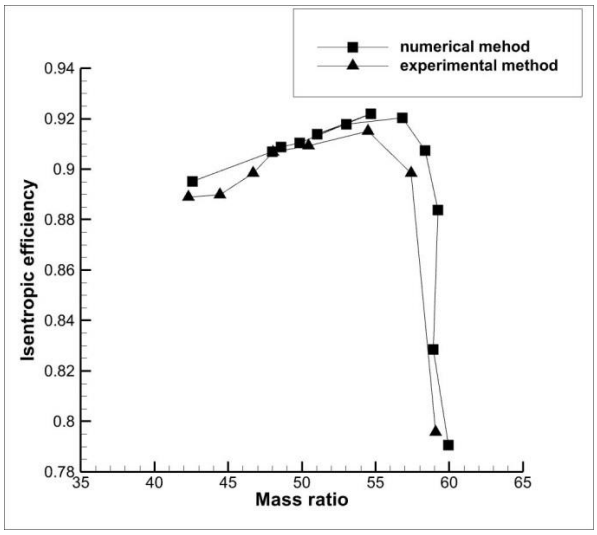

Figure 4. Comparing the isentropic efficiency of the numerical and laboratory analysis rotor at 4210 rpm.

Results and Discussion

According to Figure 5, as the flow advances in the compressor rotor, the absolute pressure increases due to the compressor performance. By moving in the horizontal axis (in the direction of the rotor chord and tandem) up to the dimensionless value of 1.3 (the main rotor blade), an increase in pressure at an approximate rate of 20% is observed; From the value of 1.3 onwards and with the start of the tandem vane effect, the pressure increase continues at a low rate (about 8%) and then stabilizes. It can be seen that the pressure increase in the main rotor part is higher than the pressure increases in the tandem part; That is, the main load is borne by the main rotor blade and the tandem blade, like a flap in the wing, has an auxiliary effect.

It can also be seen in Figure 5, with the increase in the revolution, the amount of pressure difference has also increased; The reason for this is the increase in flow rate. In general, in all rounds, the presence of tandem has increased the pressure. The effect of the tandem to the extent of more than 40% of the rotor capacity improves the pressure increase and thus the performance of the compressor. The reason for this is the increase in mass flow rate and pressure ratio. On the other hand, by controlling the vortices, the tandem blade prevents the growth of redundant vortices and has an increasing effect on the absolute Mach.

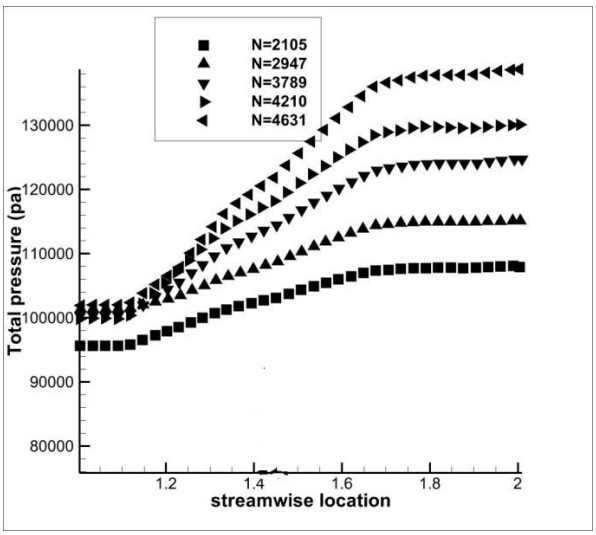

Figure 5. Diagram of static pressure in terms of dimensionless length along the chord of the rotor.

Figures 6 and 7 respectively show changes in the absolute and relative Mach according to the length of the dimensionless chord in different revolutions of the rotor. The task of the compressor is to increase the absolute pressure and speed and decrease the relative Mach number. As stated, most of the increase in absolute Mach and decrease in relative Mach is due to the main rotor and the tandem rotor is responsible for about 40% of the load. As can be seen in Figure 7, the relative Mach has decreased by advancing along the chord.

On the other hand, it can be seen in Figure 6 that the absolute Mach number goes up with the increase in the compressor revolution.

According to Figure 7, the main rotor at rated revolution reduces the Mach number by 40% and the tandem reduces the relative Mach number by 25% at its maximum effect. This decrease in the relative Mach number while passing through the tandem indicates an increase in the efficiency of the compressor and, to the same extent, an increase in the work absorption coefficient.

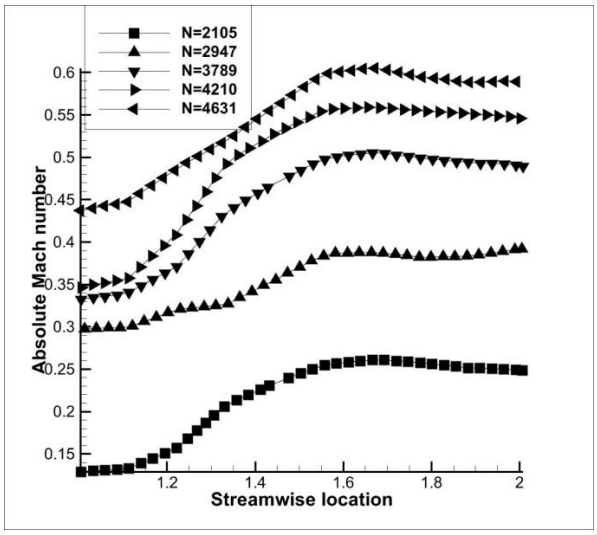

Figure 6. Absolute Mach number diagram in terms of dimensionless rotor chord length

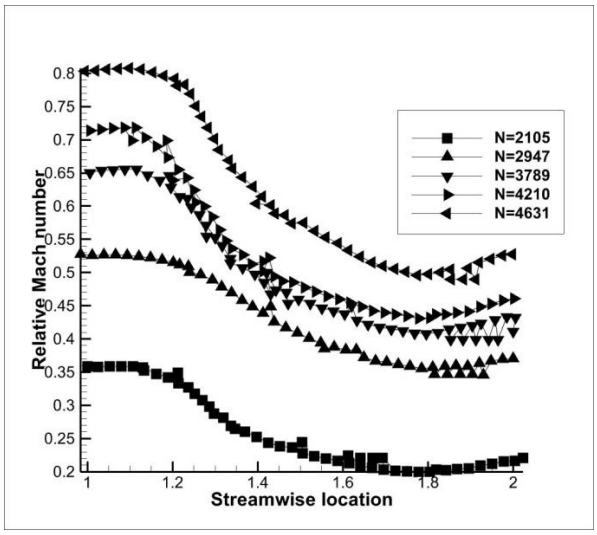

Figure 7. Relative Mach diagram in terms of dimensionless rotor chord length.

It can be seen in Figure 8, that the amount of entropy in the direction of the rotor chord increases significantly due to the presence of vortices and disturbances caused by them. Also, due to the presence of the tandem blade, the rate of entropy increase has been significantly reduced, which is due to the inhibition of the vortices and disturbances after the main rotor by the tandem blade.

Also, in Figure 8, as the compressor speed increases, the change in entropy rate increases; The reason for that is the increase in flow rate at high revolutions.

According to Figure 8, in the nominal speed and in the main rotor, the entropy increase is 8.5% and in the tandem section, this increase has reached about 2%. The noteworthy point is that the effect of the tandem was greater in lower revolutions.

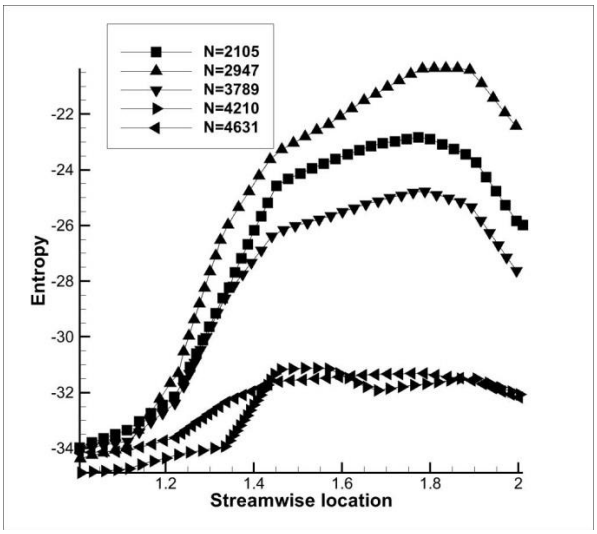

Figure 8. Entropy diagram according to the dimensionless rotor chord length

Figures 9 and 10 show the relative Mach number in terms of inlet length at the leading edge and trailing edge of the rotor, respectively. As seen in Figure 9, the relative Mach number up to the initial 80% of the inlet length shows a value of more than Mach 0.7, but after that, the value of Mach number drops to 0.2 until the end of the blade, which indicates the presence of a backward angle in the blade. Figure 10 also shows the relative Mach number at the trailing edge. in such a way that it is an ascending state up to the half inlet and after that, it is descending until approximately 0.8 of the inlet length, and then the Mach number reaches 0.3 at the end of the wing. Also, with the increase of the revolution, the amount of relative Mach number has increased in terms of the inlet length at the attack and escape edges. The reason for that is the increase in mass flow rate with the increase in revolution.

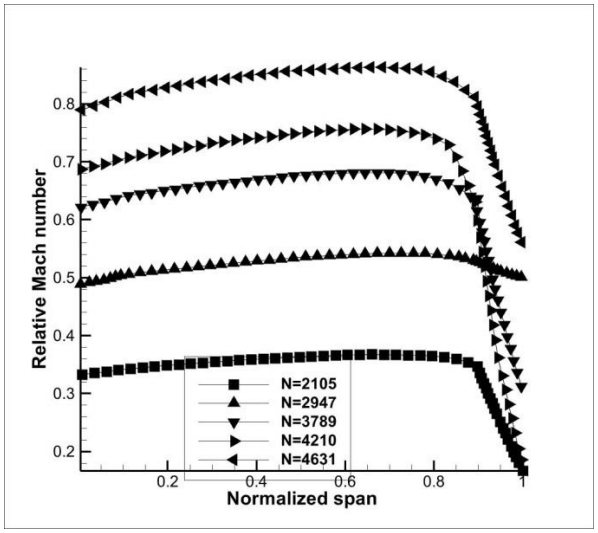

Figure 9. Plot of the relative Mach number in terms of inlet length at the leading edge of the rotor.

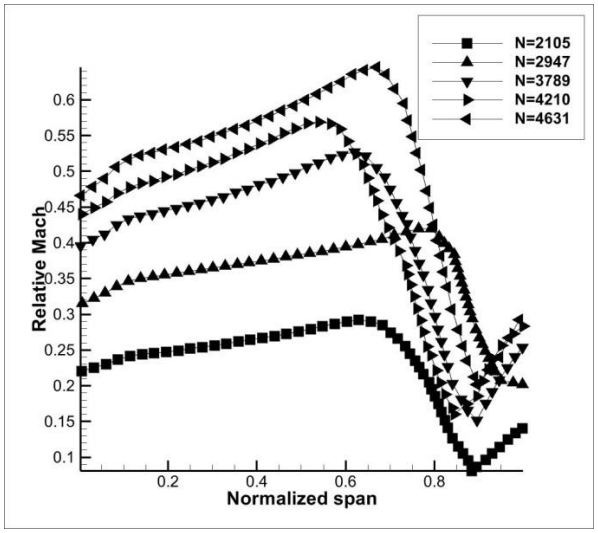

length at the trailing edge of the rotor.

Figure 11 shows the vertical velocity in terms of span length at the leading edge. As it can be seen in the figure, from the beginning of the inlet of the blade, to about half of the inlet, the vertical component of the velocity grew and then the value of vertical velocity has decreased to 0.9 of the inlet length. This speed reduction is due to the backward angle and it remains almost constant until the end of the blade.

Also, based on this figure, with the increase in the speed of the compressor, the amount of vertical revolution has also increased. The noteworthy point is that from the 0.8 section onwards, the difference in vertical speed of all revolutions is minimized.

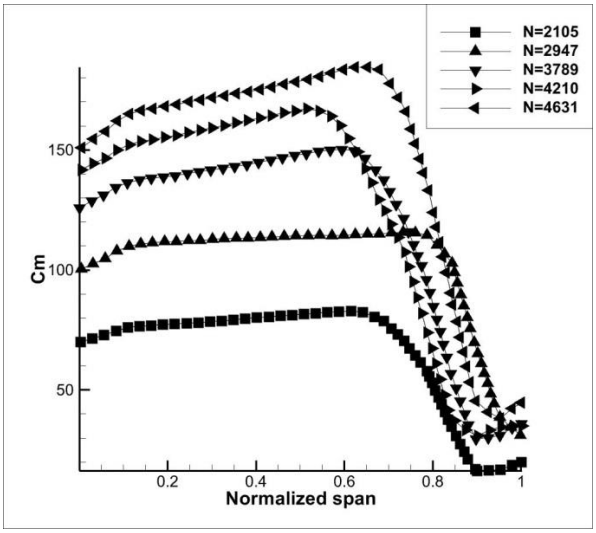

Figure 10. Plot of the vertical component of velocity in terms of span length at the leading edge of the rotor.

Figure 12 shows the relative Mach contour at the distance of 80% of the blade inlet in 3 different revolutions. It can be seen that with increasing the revolution, the vortices on the leading edge of the main rotor decrease. Also, with the increase in the revolution, the speed of the vortices after the tandem increases. Previous studies show that as the rotor revolution increases, the volume of vortices increases; But as it is known in this figure, due to the existence of tandem, the vortices behind the rotor are controlled by the tandem. It is also determined by paying attention to the post-tandem vortices with the increase in speed, the speed of the vortex core after the tandem decreases significantly, and with the increase of the compressor speed, The speed of the vortices increases after the rotor and the speed of the vortices decreases after the tandem. The reason for this is the appropriate geometry of the desired tandem in controlling the vortex and preventing the creation of unnecessary vortices.

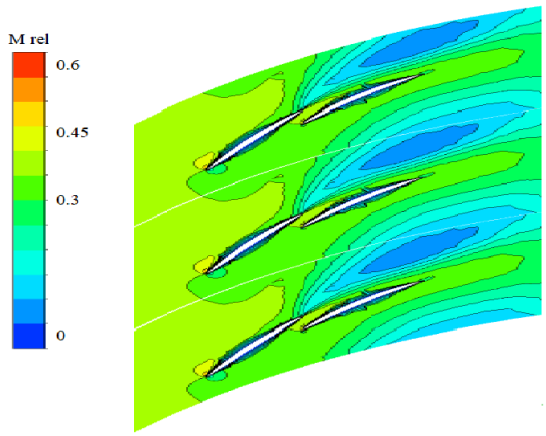

a) In 2105 RPM

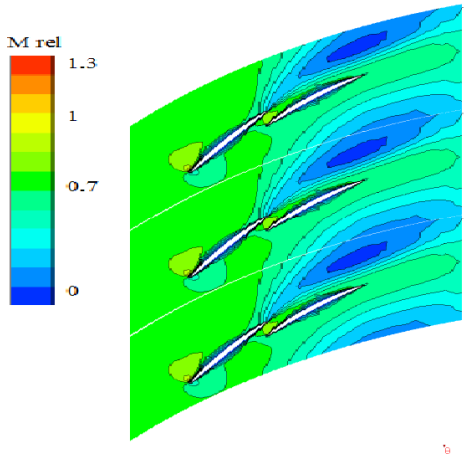

b) In 3789 RPM

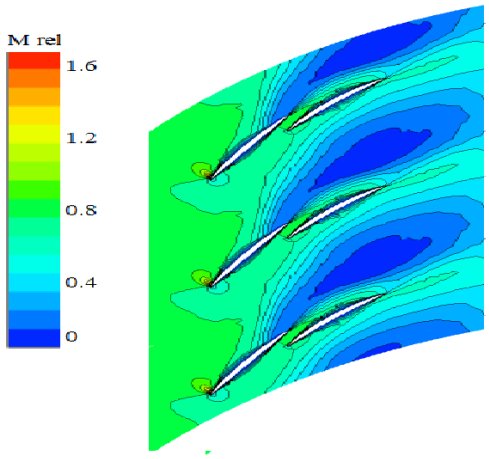

c) In 4210 RPM

Figure 11. Relative Mach contours of the rotor at the distance of 80% of the inlet.

Figure 13 shows the speed vector and contour at the distance of 80% of the inlet at different revolutions. In all figures, it is clear that the tandem actively controls the velocity vectors. Also, by carefully looking at these contours, it can be seen that the speed of the vortices after the rotor increases with the increase in the revolution. Also, the tandem controls the vortices after the rotor well.

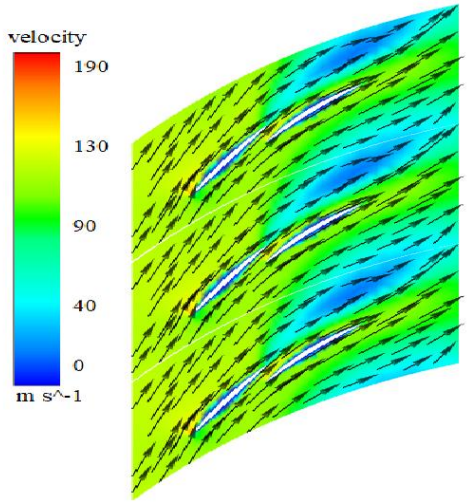

a)In 2105 RPM.

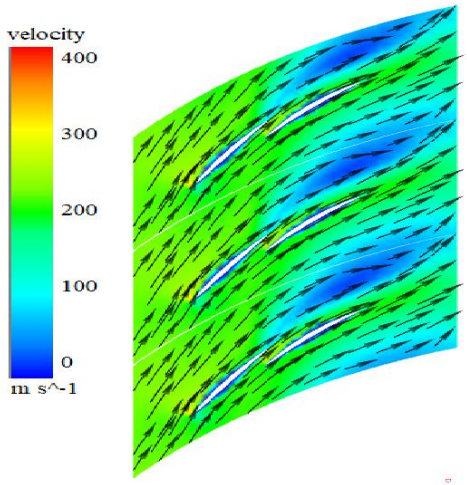

b) In 3789 RPM.

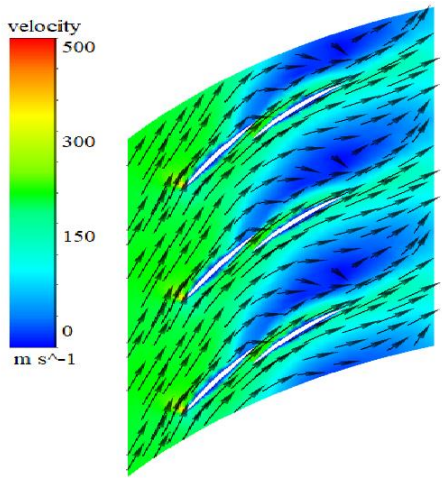

c) In 4210 RPM.

Figure 12. Rotor speed vectors at 80% chord distance

Figure 14 shows the entropy contours at the 80% chord distance for 3 different cycles. According to these figures, with the revolution increasing, the entropy value after the rotor increases significantly. It is also observed that the tandem prevents the vortex from growing after the rotor and the irrational increase of entropy.

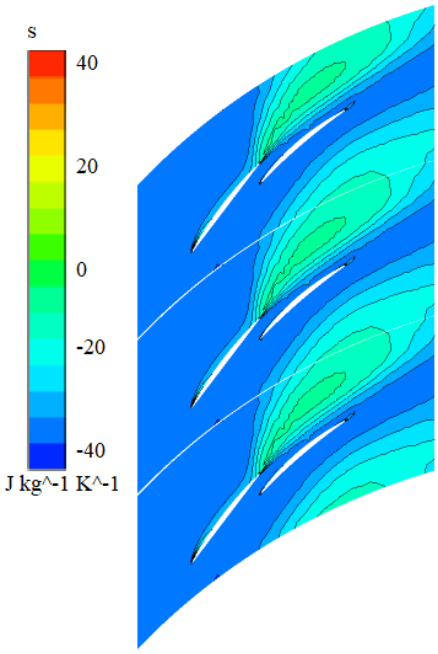

a)In 2105 RPM.

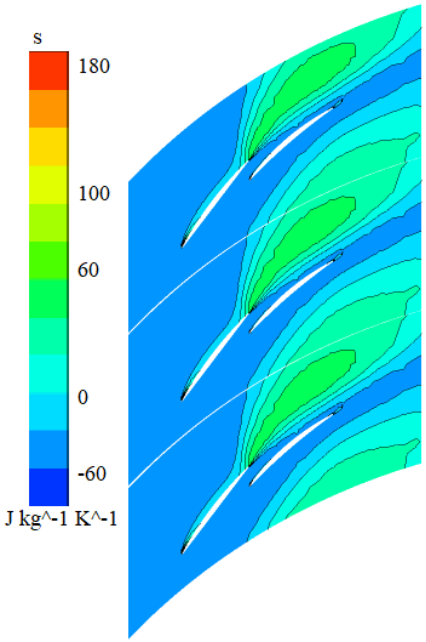

b) In 3789 RPM.

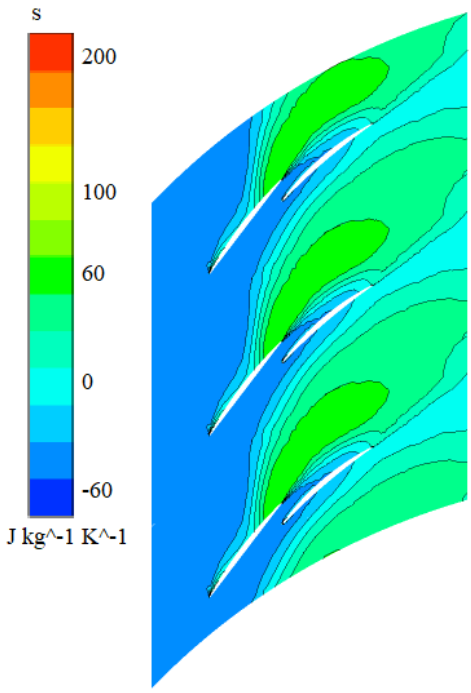

c) In 4210 RPM.

Figure 13. Rotor entropy contours at 80% inlet distance**.**

Figure 15 shows the isentropic efficiency in terms of mass flow rate. As it is clear from the figure, in some values of the flow ratio in all revolutions, the isentropic efficiency of the normal rotor is slightly higher than that of the tandem rotor. The reason for this can be the increase in friction loss; of course, this difference is not significant. It is also observed that, at the same isentropic efficiency, the tandem rotor passes more mass flow.

The isentropic efficiency ratio of the rotor is as follows:

$$\eta_{ad} = \frac{\left({}^{P_2}/_{P_1}\right)^{\frac{\gamma-1}{\gamma}} - 1}{\left(\frac{T_2}{T_1}\right) - 1} \qquad (6)$$

In the above equation, P represents the pressure and T represents the temperature.

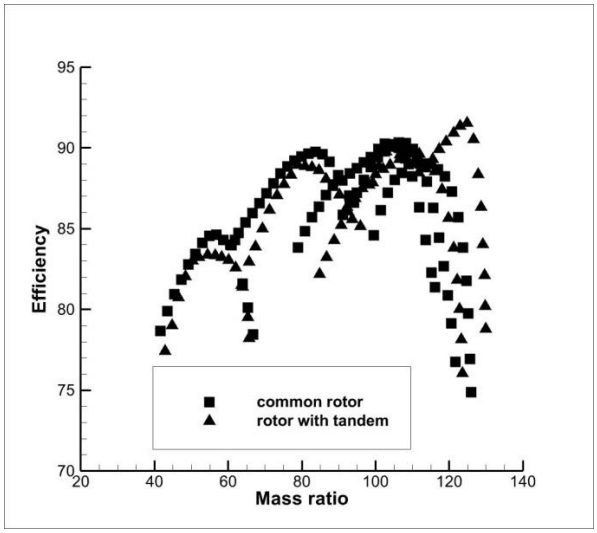

Figure 14. Comparison of isentropic efficiency in terms of mass flow rate for normal rotor and rotor with tandem.

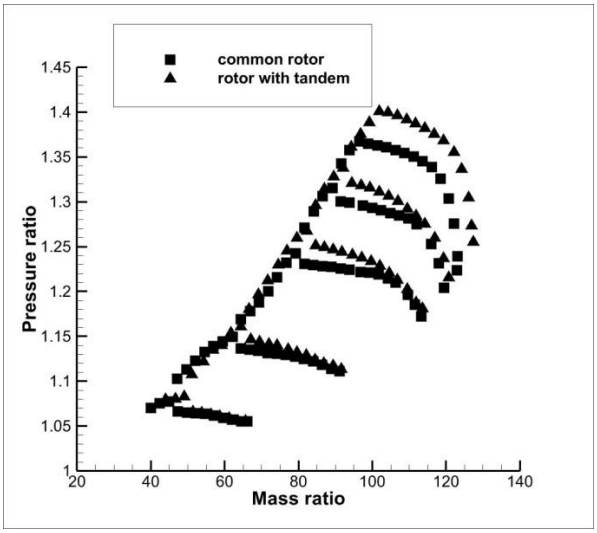

Figure 15. Comparison of pressure ratio in terms of mass flow rate for normal rotor and rotor with tandem.

The pressure ratio in terms of mass flow rate is presented in Figure 16. The reason for this is the presence of a tandem blade behind the main blade, which will increase the mass flow rate and, as a result, increase the pressure ratio. Also, the rotor surge line, up to a mass flow rate of about 65, is higher than the rotor surge line with tandem up to the mass flow rate of 88. The rotor surge line with tandem is also higher than the normal rotor surge line and from then on, both surge lines overlap. In general, it can be stated that in the design phase, the presence of tandem improves the performance line and increases the surge range and improves the compressor performance.

On the other hand, the tandem increases the compressor's absorption capacity by eliminating the extra vortices. According to Cohen-Rogers [18], compressor work absorption capacity refers to the ability of the compressor to absorb the maximum work provided by the turbine. A compressor can absorb the maximum available work, functioning at optimum operating conditions with minimal losses due to aerodynamic phenomena. The use of tandem blades in the compressor rotor improves the flow field pattern and reduces the negative effects of the separated flow and the expansion of vortices downstream of the rotor.

Conclusions

In this research, the rotor and rotor tandem of the compressor were numerically analyzed at different speeds. The obtained results show that the tandem, by controlling and restraining the vortices downstream of the rotor blade, increases the overall pressure and decreases the relative speed, thus improving the compressor performance.

By using tandem, the entropy increase rate is controlled; Because the tandem restores the flow pattern and controls the disturbances after the rotor.

This research shows that with increasing the speed, the effect of a tandem on total pressure and absolute Mach is increasing and on relative Mach and entropy growth rate is decreasing. Also, changes in the compressor revolution do not affect the alpha and beta angles at the leading and trailing edges of the rotor. As the revolution increases, the relative Mach number also increases along the length of the inlet. Calculations show that as the compressor revolution increases, the pressure ratio and isentropic efficiency also increase.

Finally, the use of tandem blades improves the aerothermodynamic performance of the compressor and increases its work absorption capacity.

Table 3. List of symbols.

C	blade chord
S	Circumferential length of blade to blade
t	Circumferential length of front blade to rear blade
X	Axial distance
AO	Axial overlap
P	Step
p	Pressure
T	Temperature
V	blade speed
u	flow rate
ω	rotational speed
N	The rotational speed of the blade in units of revolutions per minute
ρ	Density
Φ	Flow coefficient
б	The amount of rigidity
k	Thermal diffusion coefficient
μ	Dynamic viscosity coefficient
β	blade angle

References

[1] U.K. Saha, B. Roy, Experimental investigations on tandem compressor cascade performance at low speeds, Experimental Thermal and Fluid Science, Volume 14, Issue 3, 1997, Pages 263-276, ISSN 0894-1777, https://doi.org/10.1016/S0894-1777(96)00125-2.

[2] Reza Shams Aldini Lori, Abulqasem Masgarportousi, Hamza Eshraghi, Transient Numerical Analysis of Single Stage Tandem Compressor, Amirkabir Mechanical Engineering Journal, Volume 51, Number 2, 2018, Pages 399 to 411

[3] M. Eftari, H. Javaniyan, M.R. Shahhoseini, F. Ghadak ,M. Rad, Performance Modeling and Examination of Losses in the Axial -Flow Compressor, JAST. Vol. 9, No. 1, pp 75-86

[4] Carstens, V., Kemme, R., & Schmitt, S. (2003). Coupled simulation of flow-structure interaction in turbomachinery. Aerospace Science and Technology, 7, 298-306. https://doi.org/10.1016/S1270-9638(03)00016-6

[5] McGlumphy, J., Ng, W., Wellborn, S. R., and Kempf, S. (February 3, 2009). "Numerical Investigation of Tandem Airfoils for Subsonic Axial-Flow Compressor Blades." ASME. J. Turbomach. April 2009; 131(2): 021018. https://doi.org/10.1115/1.2952366

[6] McGlumphy, J., Ng, W., Wellborn, S. R., and Kempf, S. (March 25, 2010). "3D Numerical Investigation of Tandem Airfoils for a Core Compressor Rotor." ASME. J. Turbomach.July 2010;132(3): 031009. https://doi.org/10.1115/1.3149283

[7] Jonathan McGlumphy, Wing-Fai Ng, Steven R. Wellborn, Severin Kempf, 3D Numerical Investigation of Tandem Airfoils for a Core Compressor Rotor, Journal of Turbomachinery, JULY 2010.

[8] Rzadkowski, Romuald & Gnesin, V.I. & Kolodyazhnaya, Luba. (2013). Unsteady Forces Acting on Rotor Blades in Five and Half Compressor Stage. Advances in Vibration Engineering. 12. 287-301.

[9] M., Rajadurai & Mohanasundaram, R & Revathi, M & Karthikeyan, A. (2014). 3D Computational Studies of Low-Speed Axial Flow Compressor Rotor Incorporating Tandem Blades. International Journal of Engineering Research and Development. 10. 2278-800.

[10] Ahmed, Mohamed & Owis, Farouk & Hashim, Ali. (2017). The Impact of Tandem Rotor Blades on the Performance of Transonic Axial Compressors. Aerospace Science and Technology. 67. 10.1016/j.ast.2017.04.019.

[11] Pan, Ruochi & Song, Zhaoyun & Liu, Bo. (2020). Optimization Design and Analysis of Supersonic Tandem Rotor Blades. Energies. 13. 3228. 10.3390/en13123228.

[12] E. V. doroshenko, Yu. M. tereshchenko, Yu. Yu. tereshchenko, A. o. kushchinskiy, Aeroacoustics Characteristics of the Axial Compressor Stage with tandem impeller, Geotechnical and Mining Mechanical engineering, Machine Building. DOI:10.29202/nvngu/2019-1/9

[13] Baojie LIU, Chuanhai ZHANG, Guangfeng AN, Du FU, Xianjun YU, Using tandem blades to break loading limit of highly loaded axial compressors,Chinese Journal of Aeronautics, Volume 35, Issue 4, 2022,Pages 165-175, ISSN 1000-9361, https://doi.org/10.1016/j.cja.2021.07.031.

[14] Sushanlal Babu, Probuddho Chatterjee , and Pradeep A M , "Transient nature of secondary vortices in an axial compressor stage with a tandem rotor", Physics of Fluids (in press) (2022); https://doi.org/10.1063/5.0092226

[15] J. A. Brent, J. G. Cheatham, and D. R. Clemmons, single-stage experimental evaluation of tandem-airfoil rotor and stator blading for compressors, part v - analysis and design of stages d and e, december1972, pratt & whitney aircraft, division of united aircraft corporation, florida research and development center, prepared for national aeronautics and space administration, NASA Lewis Research Center, Contract NAS3-11158.

[16] Wilcox, D. C.,' Turbulence Modeling for CFD', 2nd edition ed. DCW Industries Inc., 1998.

[17] Yue, S., Wang, Y. & Wang, H. Design and Optimization of Tandem Arranged Cascade in a Transonic Compressor. J. Therm.Sci. 27, 349–358(2018). https://doi.org/10.1007/s11630-018-1013-4

[18] H. Cohen, CFC Rogers, HIH Saravanamutto, Gas Turbine Theory, Longman Group limited, 1996, P.179.